Z. Phys. B 93, 465–478 (1994)

ZEITSCHRIFT
FÜR PHYSIK B

Electron correlations and quantum lattice vibrations in strongly coupled electron-phonon systems: a variational slave boson approach

U. Trapper, H. Fehske, M. Deeg, H. Büttner

Physikalisches Institut, Universität Bayreuth, Universitätsstrasse 30, D-95440 Bayreuth, Germany

Received: 3 August 1993

Abstract. We investigate the ground-state properties of the two-dimensional Hubbard model with an additional Holstein-type electron-phonon coupling on a square lattice. The effects of quantum lattice vibrations on the strongly correlated electronic system are treated by means of a variational squeezed-polaron wave function proposed by Zheng, where the possibility of static (frozen) phonon-staggered ordering is taken into account. Adapting the Kotliar-Ruckenstein slave boson approach to the effective electronic Hamiltonian, which is obtained in the vacuum state of the transformed phonon subsystem, our theory is evaluated within a two-sublattice saddle-point approximation at arbitrary band-filling over a wide range of electron-electron and electron-phonon interaction strengths. We determine the order parameters for long-range charge and/or spin ordered states from the self-consistency conditions for the auxiliary boson fields, including an optimization procedure with respect to the variational displacement, polaron and squeezing parameters. In order to characterize the crossover from the adiabatic ($\omega=0$) to the nonadiabatic ($\omega=\infty$) regime, the frequency dependencies of these quantities are studied in detail. In the predominant charge (spin) ordered phases the static Peierls dimerization (magnetic order) is strongly reduced with increasing ω. As the central result we present the slave boson ground-state phase diagram of the Holstein-Hubbard model for finite phonon frequencies.

PACS: 63.20.Kr; 71.38.+i; 71.45.Lr; 75.30.Fv

1. Introduction

Research on the high-T_c oxide systems [1] has focused, once again, interest on strongly coupled electron-phonon (EP) systems. Whereas it is widely believed that most of the unusual normal-state properties of these materials may be related to strong electronic correlations, the importance of EP coupling is still a heavily debated issue [2]. Many experiments have indicated substantial EP coupling in the bismuthates [3, 4] and recently as well in the cuprates (cf. Raman [5] and IR data [6]). For the cuprate superconductors, ion channeling [7], neutron scattering [8] and photoinduced absorption measurements [9] also give evidence for large anharmonic lattice fluctuations, which may be responsible for local phonon-driven charge instabilities in the planar CuO_2 electron system [10, 11]. Along this line, it was suggested that polaron formation may play an important role [11–15], where in the cuprate high-T_c materials the (bi)polarons were expected to be rather "large" [16, 17]. In addition, elaborated density functional calculations [18, 19] have demonstrated that the EP coupling is strong for several modes in $Y\,Ba_2Cu_3O_7$ and $La_{2-x}(Ba, Sr)_xCuO_4$. However, the explanation of the high T_c by a phonon mechanism, i.e. the relevance of the observed strong EP interactions for the superconducting transition is still an open question both from experimental and theoretical point of view. The theoretical difficulty results from the fact that in the high-T_c materials the interaction of the charge carriers with the antiferromagnetic correlated Cu^{2+}-spin background leads to a substantial reduced characteristic energy scale for coherent motion of the dressed quasiparticles. As a consequence the EP effects become much more important in this unusual electronic environment and the standard Migdal approximation (based on $\omega_D/E_F \ll 1$) might break down [20].

The probably simplest microscopic model that can be used to address some of these issues is the Holstein-Hubbard model (HHM), which will be the main topic of the present paper. The HHM is thought to represent a narrow-band electronic system with on-site Coulomb interaction coupled locally to an optical phonon mode. In spite of the amazingly rich physics contained in the HHM, it was tailored to investigate a large variety of long-standing problems in coupled EP systems, e.g. the Peierls charge-density wave (CDW) formation [21–25], the dynamics of self-trapping transition [3] and polaron formation [26], polaronic superconductivity [15, 27] or the appearance of long-periodic (incommensurate)

phases in quasi one-dimensional (1D) systems such as MX-chain compounds [28]. Several approximative techniques have been proposed so far to deal with the Holstein-(Hubbard) Hamiltonian.

Neglecting the Coulomb interaction term, the molecular crystal, or Holstein model [29] has been investigated with respect to pairing and Peierls CDW correlations using (quantum) Monte Carlo (MC) simulations in one spatial dimension [30] and recently in two dimensions in the half-filled-band sector [31] as well as away from half-filling [32, 33]. Based on the concept "transition by breaking of analycity", Aubry et al. [34] argued that the CDW state in the Holstein model can be viewed as a superposition of bipolaronic states pinned to the lattice. The spinless Holstein model was treated by CPA [35], MC [36] and variational methods [37, 38] to discuss the self-trapping transition in the limit of low electron density ($n \ll 1$) and for the half-filled band case [39].

In the presence of Hubbard interaction U, the phase diagram of the half-filled 1D HHM was obtained from MC calculations [21]. For this model, the effects of quantum lattice fluctuations on the Peierls dimerization are worked out by means of a variational polaron wave function, where the electronic correlations are treated within the Hartree-Fock approximation [24] or using a modified Gutzwiller approach [25]. To discuss the polaronic properties in the strong EP coupling regime, a complete numerical solution was performed for the two-site HHM by Ranninger and Thibblin [68] and for an O(4)−Cu(1)−O(4) cluster Hamiltonian by Mustre de Leon et al. [13]. For the 2D HHM most of the calculations are done in the adiabatic limit ($\omega = 0$). The stability of the 2D HHM against static Peierls distortions was investigated at and near half-filling by several authors using Hartree-Fock [22], quantum MC [23] and exact diagonalization [11] methods. Lanczos diagonalization studies [11, 20, 41] of the corresponding 2D Holstein-t-J model [27, 42, 43] have demonstrated that the electronic correlations in this model can strongly enhance the probability for hole-polaron formation in the low doping regime ($n \lesssim 1$). In the course of our previous investigation of the 2D HHM, we have obtained within the slave-boson (SB) approach first results for the phase diagram of the HHM at moderate EP coupling strengths in the limit $\omega \to 0$ [44, 45]. In a subsequent paper [26], we have considered the strong EP coupling regime in order to study finite-density, squeezing and correlation effects on the polaron formation in an effective polaronic Hubbard Hamiltonian at finite phonon frequencies.

The aim of the present paper is to analyze the main features of the ground-state phase diagram of the 2D HHM by means of a detailed numerical evaluation of a variational SB technique on the saddle-point level of approximation. Our approach is based on the variational treatment of the phonon dynamics, developed by Zheng et al. [46] for the 1D half-filled Holstein model, and on the SB theory worked out by the authors for the 2D HHM in the adiabatic limit [44, 45]. The resulting theory provides an unified description of charge and/or spin ordered states compatible with the underlying bipartite lattice, where nonadiabaticity effects, e.g. polaronic band narrowing and squeezing phenomena were taken into account. With respect to Hubbard and EP interaction strengths, the variational SB scheme allows an interpolation between weak and strong coupling regimes as well as between adiabatic and antiadiabatic limits. For the first time, we discuss the interplay of dimerization and polaronic effects as a function of band-filling.

In the numerical work, however, we will limit ourselves to the case of moderate EP coupling, where we obtain a weak mass renormalisation, i.e. light polarons. The case of self-trapped heavy polarons, which is realized only at extreme EP coupling strengths, was studied within a paramagnetic version of the present theory by Fehske et al. [26]. In addition, we will restrict our calculations to the normal state properties of the HHM, and do not allow for incommensurate charge or spin structures.

The plan of this paper is as follows: In Sect. 2.1. we briefly discuss the essential features of the Holstein-Hubbard Hamiltonian and, in particular, the relevant energy scales for the different model parameters. Section 2.2. then proceeds to present the variational treatment of the phonon subsystem. Our trial wave function contains variational parameters related to static phonon ordering and to squeezed polaronic effects [25, 26]. Taking the average on the phonon vacuum the effective electronic problem is treated in Sect. 2.3. in terms of slave bosons à la Kotliar and Ruckenstein [47]. The self-consistency equations for the SB fields are derived using a two-sublattice saddle-point approximation in the functional integral representation of the partition function. Accordingly, the extremal requirements that are imposed on the variational parameters then can be obtained by minimizing the corresponding SB free-energy functional. A detailed numerical analysis of the theory developed in Sect. 2 is carried out in Sect. 3 in order to obtain the ground-state phase diagram of the HHM. In addition some important limiting cases will be studied in this section, e.g. the half-filled band case, the adiabatic and antiadiabatic limits, or the pure Holstein model. Finally, we summarize the main results and discuss the limits of validity of the present approach in Sect. 4.

2. Theoretical analysis of the 2D Holstein-Hubbard model

2.1. *The model*

The starting point of our work is the single-band Holstein-Hubbard Hamiltonian

$$\mathcal{H} = \mathcal{H}_{el} + \mathcal{H}_{el-ph} + \mathcal{H}_{ph}, \tag{2.1}$$

with

$$\mathcal{H}_{el} = -t \sum_{\langle ij \rangle \sigma} (c_{i\sigma}^{\dagger} c_{j\sigma} + \text{H.c.}) + U \sum_{i} n_{i\uparrow} n_{i\downarrow}, \tag{2.2}$$

$$\mathcal{H}_{el-ph} = -\lambda \sum_{i\sigma} q_i n_{i\sigma}, \tag{2.3}$$

$$\mathcal{H}_{ph} = \sum_{i} \left(\frac{p_i^2}{2M} + \frac{K}{2} q_i^2 \right). \tag{2.4}$$

The first term represents the standard Hubbard model, where $c_{i\sigma}^{\dagger}(c_{i\sigma})$ denote the creation (annihilation) operators for spin σ electrons at Wannier site i, and $n_{i\sigma}=c_{i\sigma}^{\dagger}c_{i\sigma}$. The transfer matrix element t is restricted to nearest neighbour $\langle ij\rangle$ hopping processes on a 2D square lattice, and U is the on-site part of the Coulomb interaction. The second term couples the electronic system via the EP interaction constant λ locally to an internal optical degree of freedom of the effective lattice i. $\mathscr{H}_{ph}$ takes into account the elastic energy of a harmonic lattice with spring constant K and mass M. In the context of the copper-oxide planes of, e.g., $La_{2-x}Ba_xCuO_4$ the Holstein coordinates takes the form

$$q_i=(x_{i_x,i_y}-x_{i_x-1,i_y}+y_{i_x,i_y}-y_{i_x,i_y-1})/4, \tag{2.5}$$

for in-plane oxygen breathing modes [22, 23, 44, 45], where the bond-parallel displacements of both oxygens in the unit cell $i=(i_x,i_y)$ are related by $x_{i_x,i_y}=-x_{i_x-1,i_y}=y_{i_x,i_y}=-y_{i_x,i_y-1}$. At half-filling the EP coupling may lead to a Peierls instability (in competition to the AFM instability triggered by U), which is connected to a static (π,π) distortion of the square lattice (frozen phonon mode). The model (2.1) could be easily extended to the inclusion of out-of-plane (apical) oxygen vibrations [11].

In terms of K and M we define a reference phonon frequency $\omega=\sqrt{K/M}$. Introducing as usual phonon creation $b_i^{\dagger}$ and destruction operators b_i

$$p_i=i\sqrt{\frac{\hbar\omega M}{2}}(b_i^{\dagger}-b_i) \tag{2.6a}$$

$$q_i=\sqrt{\frac{\hbar}{2M\omega}}(b_i^{\dagger}+b_i). \tag{2.6b}$$

for a quantum mechanical description of lattice vibrations, the Hamiltonian (2.1) transforms to

$$\mathscr{H}=\hbar\omega\sum_{i\sigma}(b_i^{\dagger}b_i+\tfrac{1}{2})-\sqrt{\hbar\omega\varepsilon_p}\sum_i(b_i^{\dagger}+b_i)n_{i\sigma} -t\sum_{\langle ij\rangle\sigma}(c_{i\sigma}^{\dagger}c_{j\sigma}+\text{H.c.})+U\sum_i n_{i\uparrow}n_{i\downarrow}, \tag{2.7}$$

where $\varepsilon_p=\lambda^2/2K$.

The physics of the HHM is governed by three competing effects: the itinerancy of the electrons, their Coulomb repulsion and the local EP interaction. Once the energy scale has been extracted, there are two dimensionless ratios of energies, U/t and ε_p/t, which mainly determine the tendency of the itinerant quantum-mechanical system to establish a magnetic or charge ordered state, respectively. Since, however, the EP coupling is retarded in nature, the ratio between phonon frequency and electronic hopping amplitude $\hbar\omega/t$ defines a third relevant energy scale of the problem. Obviously, the significance of the different effects depends on the electron density n, which is the fourth crucial parameter involved in the HHM.

For the pure (1D) Holstein-model, the different energy regimes and the corresponding approximations were recently classified by Feinberg et al. [39] in terms of ε_p/t, $\hbar\omega/t$, and $\sqrt{\varepsilon_p/\hbar\omega}$. The condition $\varepsilon_p/t>1(<1)$ refers to the strong (weak) coupling case. On the other hand $\sqrt{\varepsilon_p/\hbar\omega}>1(<1)$ means that multiphonon (single phonon) processes are involved in the electron dynamics [39]. The adiabatic regime is then characterized by the relations $\hbar\omega\ll t$, ε_p and $\sqrt{\hbar\omega\varepsilon_p}\ll t$, i.e., if $t<\sqrt{\hbar\omega\varepsilon_p}$ is fulfilled, non-adiabatic effects becomes important even for $\hbar\omega<t$ [39]. The non-adiabatic strong-coupling case may lead to polaron formation and, provided an attractive interaction is induced, to polaronic or bipolaronic superconductivity [3, 48]. In the opposite adiabatic limit, the competition between CDW states and standard BCS-like superconductivity takes place.

As mentioned above, the situation becomes much more complicated if the Coulomb correlations are taken into account. Especially near half-filling the interplay between electron-electron and EP interactions may drive the system further to the strongly correlated regime. From this point of view it seems highly desirable to develop and analytical approach which allows for the description of the aforementioned limiting cases in the framework of a unified theory. This is especially important for an understanding of the intermediated region, where the energy scales are not well separated.

2.2. *Variational treatment of the phonon subsystem*

Let us now set up an effective Hamiltonian for the HHM. We begin by constructing a variational ground state.

$$|\Psi_V\rangle=\mathscr{U}(|\Psi_p\rangle\otimes|\Psi_e\rangle) \tag{2.8a}$$

$$\mathscr{U}=e^{-S_1(\Delta)}e^{-S_2(\bar{\gamma},\gamma)}e^{-S_3(\alpha)}, \tag{2.8b}$$

based on a unitary transformation $\mathscr{U}$, which contains different variational parameters Δ, $\bar{\gamma}$, γ and α. The ansatz (2.8) decouples the *transformed* phonon and electron subsystems described by

$$\tilde{\mathscr{H}}=\mathscr{U}^{\dagger}\mathscr{H}\mathscr{U}. \tag{2.9}$$

Considering ground-state properties, one obtains the effective electronic Hamiltonian by taking the average of $\tilde{\mathscr{H}}$ on the new phonon vacuum state $|\Psi_p^0\rangle$, i.e. $\mathscr{H}_{\text{eff}}\equiv\langle\Psi_p^0|\tilde{\mathscr{H}}|\Psi_p^0\rangle$. The variational parameters are then adjusted by minimization of the ground-state energy $\langle\Psi_e^0|\mathscr{H}_{\text{eff}}|\Psi_e^0\rangle$.

Following the approach of Zheng et al. [46] we perform first a coherent-state transformation

$$S_1(\Delta)=-\frac{\Delta}{2\sqrt{\hbar\omega\varepsilon_p}}\sum_i(-1)^i(b_i^{\dagger}-b_i), \tag{2.10}$$

which introduces the variational parameter Δ as a measure of static phonon-staggered ordering (related to a frozen-in (π,π) dimerization of the square lattice). This effect should be of special importance near half-filling in the adiabatic limit. To describe polaronic effects at arbitrary band fillings, we use a modified variational Lang-Firsov transformation (MVLF)

$$S_2(\bar{\gamma},\gamma)=-\sqrt{\frac{\varepsilon_p}{\hbar\omega}}\sum_{i\sigma}\left(\frac{\bar{\gamma}}{2}+\gamma n_{i\sigma}\right)(b_i^\dagger-b_i), \tag{2.11}$$

where γ measures the degree of the polaron effect ($0<\gamma\leqq 1$), which in the standard polaron theories [37, 49] becomes most important within the domain of validity of the Holstein approximation [29, 39], i.e. for $t\ll\hbar\omega$, $\sqrt{\varepsilon_p\hbar\omega}$ and $n\ll 1$. For $\gamma\equiv 1$ and $\bar{\gamma}\equiv 0$, S_2 becomes the well-known Lang-Firsov transformation [49]. Minimization of the ground-state energy with respect to $\bar{\gamma}$ yields $\bar{\gamma}=n-\gamma n$ (see Sect. 2.3.2). Thus in S_2, the first term results in a mean shift of the equilibrium position of the local oscillators, where the second term couples the polaronic distortion to the density fluctuation n_i-n. As was shown by Fehske et al. [26], the transformation (2.11) describes finite-density effects much more correctly than the variational Lang-Firsov approach ($\bar{\gamma}\equiv 0$) used by Feinberg et al. [39].

Next, to take into account for the anharmonicity of the phonon modes we perform the squeezing transformation proposed by Zheng et al. [46, 50]

$$S_3(\alpha)=-\alpha\sum_i(b_i^\dagger b_i^\dagger-b_i b_i) \tag{2.12}$$

generating a new type of Glauber coherent lattice states, the two-phonon state [51]. The squeezing effect, which becomes relevant at finite electron densities, counteracts the polaronic band narrowing. The inclusion of squeezing phenomena is a first step towards the understanding of the multiphonon regime at intermediate coupling strengths, where $1\lesssim\varepsilon_p/t<\sqrt{\varepsilon_p/\hbar\omega}$. More recently, the squeezing approach has been generalized by taking into account the correlations between different squeezed phonon states [52].

As a result of (2.8) with (2.10) to (2.12), the transformed Hamiltonian (2.9) is given by

$$\begin{aligned}\tilde{\mathscr{H}}=&\frac{\Delta^2 N}{4\varepsilon_p}+\bar{\gamma}^2\varepsilon_p N\\&+\frac{\hbar\omega}{2}(\tau^2+\tau^{-2})\sum_i(b_i^\dagger b_i+\tfrac{1}{2})\\&+\frac{\hbar\omega}{4}(\tau^2-\tau^{-2})\sum_i(b_i^\dagger b_i^\dagger+b_i b_i)\\&+\frac{\Delta}{2}\sqrt{\frac{\hbar\omega}{\varepsilon_p}}\tau^{-1}\sum_i(-1)^i(b_i^\dagger+b_i)\\&+\sqrt{\hbar\omega\varepsilon_p}\,\bar{\gamma}\tau^{-1}\sum_i(b_i^\dagger+b_i)\\&-\Delta(1-\gamma)\sum_{i\sigma}(-1)^i n_{i\sigma}-\sqrt{\hbar\omega\varepsilon_p}(1-\gamma)\\&\cdot\tau^{-1}\sum_{i\sigma}(b_i^\dagger+b_i)n_{i\sigma}\\&-\varepsilon_p[2\gamma-\gamma^2+2(1-\gamma)\bar{\gamma}]\sum_{i\sigma}n_{i\sigma}\\&+[U-2\varepsilon_p(2\gamma-\gamma^2)]\sum_i n_{i\uparrow}n_{i\downarrow}\\&-t\sum_{\langle ij\rangle\sigma}\left(\exp\left\{-\gamma\tau\sqrt{\frac{\varepsilon_p}{\hbar\omega}}[(b_i^\dagger-b_j^\dagger)-(b_i-b_j)]\right\}\right.\\&\left.\cdot c_{i\sigma}^\dagger c_{j\sigma}+\text{H.c.}\right),\end{aligned} \tag{2.13}$$

where the squeezing parameter $\tau^2=\exp\{-4\alpha\}$ was introduced. Taking the average over the state $|\Psi_p^0\rangle$, we get the effective Hamiltonian

$$\begin{aligned}\mathscr{H}_{\text{eff}}=&\frac{\Delta^2 N}{4\varepsilon_p}+\bar{\gamma}^2\varepsilon_p N+\frac{\hbar\omega N}{4}(\tau^2+\tau^{-2})\\&-\Delta(1-\gamma)\sum_{i\sigma}(-1)^i n_{i\sigma}\\&-\varepsilon_p[2\gamma-\gamma^2+2(1-\gamma)\bar{\gamma}]\sum_{i\sigma}n_{i\sigma}\\&+[U-2\varepsilon_p(2\gamma-\gamma^2)]\sum_i n_{i\uparrow}n_{i\downarrow}\\&-t\rho\sum_{\langle ij\rangle\sigma}(c_{i\sigma}^\dagger c_{j\sigma}+\text{H.c.}).\end{aligned} \tag{2.14}$$

Here

$$\rho=\exp\{-\varepsilon_p\gamma^2\tau^2/\hbar\omega\} \tag{2.15}$$

is the polaronic band narrowing factor, where, for $\gamma^2=\tau^2=1$, ε_p denotes the small-polaron binding energy in the atomic limit $t=0$. Note that the transformed phonon vacuum is not an eigenstate of the phonon number operators. Since the generators S_1 and S_2 do not commute with S_3, the variational state $|\Psi_V\rangle$ with minimal uncertainty was obtained in applying first the squeezing transformation [39]. As can be seen from the third term of $\mathscr{H}_{\text{eff}}(\Delta,\bar{\gamma},\gamma,\tau^2)$, the squeezing transformation leads via a frequency renormalization to an increase of the zero-point energy of the phonons. On the other hand, the reduction of the hopping integral is weakened by τ^2 (and, in addition, for $\gamma^2<1$), i.e. the phonon squeezing decreases the zero-point fluctuations of the conjugated momentum. Therefore one can expect a maximal squeezing effect somewhere between the weak and strong coupling limits [39]. With respect to the interplay of the dynamic polaron effect and the static CDW formation, Zheng's approach [46, 50] incorporates the interference of both contributions (cf. the fourth term of (2.14)). This effect was ommited in the variational treatment of Nasu [53]. Finally, in H_{eff}, the bare Hubbard repulsion becomes renormalized ($U\to U_{\text{eff}}=U-2\varepsilon_p(2\gamma-\gamma^2)$), which raises the probability of a phonon induced attractive interaction $U_{\text{eff}}<0$.

2.3. *Slave boson theory for the effective electronic Hamiltonian*

2.3.1. *Slave boson representation of $\mathscr{H}_{\text{eff}}$.* In order to treat the correlation effects incorporated in the effective model (2.14) in a nonperturbative way, we use a slave-boson approach [54] in the formulation introduced by Kotliar and Ruckenstein [47]. Their SB scheme provides a sym-

metric representation of spin and charge degrees of freedom [55] and should therefore be an appropriate starting point for a treatment of the HHM as well. Since a detailed presentation of the SB theory applied to the static HHM has been given by the authors in [45], we restrict us to list the essential steps and equations.

Following Kotliar and Ruckenstein [47], the original electron operators of our model (2.14) are substituted according to

$$\begin{aligned} &n_{i\uparrow}\, n_{i\downarrow} \to d_i^\dagger\, d_i \\ &n_{i\sigma} \to \tilde{n}_{i\sigma} \\ &c_{i\sigma}^\dagger\, c_{j\sigma} \to \tilde{c}_{i\sigma}^\dagger\, \tilde{c}_{j\sigma}\, z_{i\sigma}^\dagger\, z_{j\sigma}, \end{aligned} \tag{2.16}$$

where the projectors

$$\begin{aligned} z_{i\sigma} = &(1-d_i^\dagger\, d_i - p_{i\sigma}^\dagger\, p_{i\sigma})^{-\frac{1}{2}} (e_i^\dagger\, p_{i\sigma} + p_{i-\sigma}^\dagger\, d_i) \\ &\cdot (1-e_i^\dagger\, e_i - p_{i-\sigma}^\dagger\, p_{i-\sigma})^{-\frac{1}{2}} \end{aligned} \tag{2.17}$$

are introduced to ensure the correct $U=0$ limit at the mean-field level. To eliminate the unphysical states in the enlarged Fock space, the four auxiliary boson fields $e_i^{(\dagger)}$, $p_{i\sigma}^{(\dagger)}$ and $d_i^{(\dagger)}$ (which refer to the empty, single occupied σ and doubly occupied site i, respectively) are enslaved to the pseudo-fermion fields $\tilde{c}_{i\sigma}^{(\dagger)}$ by a set of local constraints:

$$Q_i^{(1)} = e_i^\dagger\, e_i + \sum_\sigma p_{i\sigma}^\dagger\, p_{i\sigma} + d_i^\dagger\, d_i - 1 = 0 \tag{2.18a}$$

$$Q_{i\sigma}^{(2)} = \tilde{c}_{i\sigma}^\dagger\, \tilde{c}_{i\sigma} - p_{i\sigma}^\dagger\, p_{i\sigma} - d_i^\dagger\, d_i = 0. \tag{2.18b}$$

Then, in the physical subspace, the resulting SB-Hamiltonian

$$\begin{aligned} \mathscr{H}_{\text{eff}}^{\text{SB}} = &N\left[\frac{\hbar\omega}{4}(\tau^2+\tau^{-2}) + \frac{\Delta^2}{4\varepsilon_p} + \bar{\gamma}^2\, \varepsilon_p\right] \\ &-\sum_{i\sigma}\{\varepsilon_p[2\gamma-\gamma^2+2(1-\gamma)\,\bar{\gamma}] \\ &+(-1)^i\, \Delta(1-\gamma)\}\, \tilde{n}_{i\sigma} \\ &+[U-2\varepsilon_p(2\gamma-\gamma^2)] \sum_i d_i^\dagger\, d_i \\ &-t\rho \sum_{\langle ij\rangle\sigma} (\tilde{c}_{i\sigma}^\dagger\, \tilde{c}_{j\sigma}\, z_{i\sigma}^\dagger\, z_{j\sigma} + \text{H.c.}) \end{aligned} \tag{2.19}$$

has the same matrix elements as $\mathscr{H}_{\text{eff}}$. The grand canonical partition function for the model (2.19) can be expressed as coherent state functional integral over Grassmann fermion and complex boson fields [56]

$$\begin{aligned} \mathscr{Z} = &\int \mathscr{D}[\tilde{c}_\sigma^*, \tilde{c}_\sigma]\, \mathscr{D}[e^*, e] \\ &\mathscr{D}[p_\sigma^*, p_\sigma]\, \mathscr{D}[\mathrm{d}^*, \mathrm{d}]\, \mathrm{d}[\lambda_i^{(1)}]\, \mathrm{d}[\lambda_{i\sigma}^{(2)}] \exp\{\mathscr{S}_{\text{eff}}^{\text{SB}}\}, \end{aligned} \tag{2.20}$$

with the action

$$\begin{aligned} \mathscr{S}_{\text{eff}}^{\text{SB}} = &\beta N\left[\frac{\hbar\omega}{4}(\tau^2+\tau^{-2}) + \frac{\Delta^2}{4\varepsilon_p} + \bar{\gamma}^2\, \varepsilon_p\right] \\ &+\int_0^\beta \mathrm{d}\tau' \sum_i \{e_i^*\, \partial_{\tau'}\, e_i + d_i^*\, \partial_{\tau'}\, d_i \\ &+\sum_\sigma \tilde{c}_{i\sigma}^*(\partial_{\tau'}-\mu)\, \tilde{c}_{i\sigma} + \sum_\sigma p_{i\sigma}^*\, \partial_{\tau'}\, p_{i\sigma} \\ &+\lambda_i^{(1)}(e_i^*\, e_i + \sum_\sigma p_{i\sigma}^*\, p_{i\sigma} + d_i^*\, d_i - 1) \\ &+\sum_\sigma \lambda_{i\sigma}^{(2)}(\tilde{c}_{i\sigma}^*\, \tilde{c}_{i\sigma} - p_{i\sigma}^*\, p_{i\sigma} - d_i^*\, d_i) \\ &-\sum_\sigma \tilde{c}_{i\sigma}^*\{\varepsilon_p[2\gamma-\gamma^2+2(1-\gamma)\,\bar{\gamma}] \\ &+(-1)^i\, \Delta(1-\gamma)\}\, \tilde{c}_{i\sigma} \\ &+[U-2\varepsilon_p(2\gamma-\gamma^2)]\, d_i^*\, d_i \\ &-t\rho \sum_{j(\neq i),\sigma} (\tilde{c}_{i\sigma}^*\, \tilde{c}_{j\sigma}\, z_{i\sigma}^*\, z_{j\sigma} + \text{H.c.})\}. \end{aligned} \tag{2.21}$$

Here μ is the chemical potential, β is the inverse temperature and the constraints are incorporated by an integral representation of the δ-function [45] which naturally introduces the Lagrange multipliers $\{\lambda_i^{(1)}\}$ and $\{\lambda_{i\sigma}^{(2)}\}$.

For the Hubbard model in the absence of symmetry-breaking phases, the paramagnetic saddle-point approximation of the functional integral (2.20) was shown to be equivalent to the Gutzwiller variational approach. Compared to the Gutzwiller treatment of the 1D HHM [25], the present scheme has the main advantage that it can be easily generalized to include magnetic ordered states, e.g. antiferro- (AFM), ferro- (FM), and ferrimagnetic (FIM) phases [45] or, using a spin-rotation invariant formulation [57], even incommensurate spiral magnetic structures [58]. Furthermore, the approach offers an excellent starting point in performing loop expansions around the saddle-point solution (for the pure Hubbard model see [59]).

2.3.2. *Two-sublattice saddle point approximation.* To proceed, we can make use of the $U(1)^{\otimes 3}$ gauge freedom of the action (2.21) to transform the Lagrange multipliers into bose fields and remove three bosonic phases in the so-called radial gauge [45, 55, 59]. Performing the Gaussian integrals over the fermionic Grassmann fields, one obtains an exact bosonic representation of the partion function for our effective model (2.14). Since an unrestricted minimization of the corresponding free energy functional is impossible, we evaluate the theory at the saddle-point level where all bose fields become real variables. Due to the bipartite structure of the square lattice, we will further adopt the two-sublattice mean field approximation [60], i.e. the bose fields are considered as static and uniform on a sublattice $\eta = A, B$ which also implies that the constraints (2.18) are satisfied on each sublattice only on average. This approximation allows for a description of the paramagnetic (polaronic) phase and of long-range ordered states such as FM, AFM, and FIM with or without a (π, π) CDW (dimerization). The perfect Fermi surface nesting of 2D tight-binding band structure $\varepsilon_{\mathbf{k}} = -2t(\cos k_x + \cos k_y)$ points towards the occurence of A–B symmetry broken states at least at half-filling.

Then the free energy per site can be represented as

$$\begin{aligned} f(\Delta, \bar{\gamma}, \gamma, \tau^2) = &\frac{\hbar\omega}{4}(\tau^2+\tau^{-2}) + \frac{\Delta^2}{4\varepsilon_p} + \bar{\gamma}^2\, \varepsilon_p + \mu n \\ &+\frac{1}{2}\sum_\eta \{-\lambda_\eta^{(1)} + \lambda_\eta^{(1)}\, e_\eta^2 \end{aligned}$$

$$+\sum_{\sigma}(\lambda_{\eta}^{(1)}-\lambda_{\eta\sigma}^{(2)})\,p_{\eta\sigma}^{2}$$
$$+[\lambda_{\eta}^{(1)}-\sum_{\sigma}\lambda_{\eta\sigma}^{(2)}+U-2\varepsilon_p(2\gamma-\gamma^2)]\,d_{\eta}^{2}\}$$
$$+\frac{1}{\beta N}\sum_{\mathbf{k}\nu\sigma}\ln\{1-n_{\mathbf{k}\nu\sigma}\}, \tag{2.22}$$

where

$$n_{\mathbf{k}\nu\sigma}=\frac{1}{\exp\{\beta(E_{\mathbf{k}\nu\sigma}-\mu)\}+1} \tag{2.23}$$

holds, and the quasiparticle energies ($\nu=\pm1$)

$$E_{\mathbf{k}\nu\sigma}=\lambda_{\sigma}^{(+)}-\varepsilon_p[2\gamma-\gamma^2+2(1-\gamma)\,\bar{\gamma}]+\varepsilon_{\mathbf{k}\nu\sigma} \tag{2.24a}$$
$$\varepsilon_{\mathbf{k}\nu\sigma}=\nu\sqrt{(\lambda_{\sigma}^{(-)}-\Delta(1-\gamma))^2+\rho^2\,q_{A\sigma}\,q_{B\sigma}\,\varepsilon_{\mathbf{k}}^2}. \tag{2.24b}$$

are obtained by diagonalizing the fermionic matrix. Here, we have introduced the correlation-induced band narrowing factor $q_{\eta\sigma}=|z_{\eta\sigma}|^2$ and the notation $\lambda_{\sigma}^{(\pm)}:=(\lambda_{A\sigma}^{(2)}\pm\lambda_{B\sigma}^{(2)})/2$. Note that the $\mathbf{k}$-summation is restricted to the magnetic Brillouin zone of the square lattice. At given electron density n, the chemical potential μ is fixed by the requirement

$$n=(1-\delta)=\frac{1}{N}\sum_{\mathbf{k}\nu\sigma}n_{\mathbf{k}\nu\sigma}, \tag{2.25}$$

where δ denotes the deviation from half-filled band case.

Requiring the free energy functional (2.22) to be stationary with respect to variations of the bosonic fields e_η, d_η, $p_{\eta\sigma}$, $\lambda_{\eta}^{(1)}$, and $\lambda_{\eta\sigma}^{(2)}$, one has to solve the set of 14 coupled saddle-point equations

$$\lambda_{\eta}^{(1)}\,e_{\eta}=\sum_{\sigma'}q_{-\eta\sigma'}\frac{4x_{\eta\sigma'}}{1-4\delta_{\eta\sigma'}^2}\left(\frac{2e_{\eta}\,x_{\eta\sigma'}}{1+2\delta_{\eta\sigma'}}-p_{\eta\sigma'}\right)\rho^2\,I_{\sigma'}^{(2)}, \tag{2.26a}$$

$$[\lambda_{\eta}^{(1)}-\sum_{\sigma}\lambda_{\eta\sigma}^{(2)}+U-2\varepsilon_p(2\gamma-\gamma^2)]\,d_{\eta}$$
$$=\sum_{\sigma'}q_{-\eta\sigma'}\frac{4x_{\eta\sigma'}}{1-4\delta_{\eta\sigma'}^2}\left(\frac{2d_{\eta}\,x_{\eta\sigma'}}{1-2\delta_{\eta\sigma'}}-p_{\eta-\sigma'}\right)\rho^2\,I_{\sigma'}^{(2)}, \tag{2.26b}$$

$$[\lambda_{\eta}^{(1)}-\lambda_{\eta\sigma}^{(2)}]\,p_{\eta\sigma}$$
$$=\sum_{\sigma'}q_{-\eta\sigma'}\frac{4x_{\eta\sigma'}}{1-4\delta_{\eta\sigma'}^2}\left[\left(\frac{2p_{\eta\sigma'}\,x_{\eta\sigma'}}{1-2\delta_{\eta\sigma'}}-e_{\eta}\right)\delta_{\sigma\sigma'}\right.$$
$$\left.+\left(\frac{2p_{\eta-\sigma'}\,x_{\eta\sigma'}}{1+2\delta_{\eta\sigma'}}-d_{\eta}\right)\delta_{\sigma-\sigma'}\right]\rho^2\,I_{\sigma'}^{(2)}, \tag{2.26c}$$

$$e_{\eta}^2+d_{\eta}^2+\sum_{\sigma}p_{\eta\sigma}^2=1 \tag{2.26d}$$

$$d_{\eta}^2+p_{\eta\sigma}^2=\frac{1}{N}\sum_{k\nu}n_{k\nu\sigma}\left(1+\xi_{\eta}\frac{\lambda_{\sigma}^{(-)}-\Delta(1-\gamma)}{\varepsilon_{\mathbf{k}\nu\sigma_{\varepsilon}}}\right) \tag{2.26e}$$

self-consistently with the following extremal equations for the variational parameters Δ, $\bar{\gamma}$, γ, and τ^2:

$$\Delta=2\varepsilon_p(1-\gamma)\sum_{\sigma}[\lambda_{\sigma}^{(-)}-\Delta(1-\gamma)]\,I_{\sigma}^{(0)} \tag{2.27a}$$

$$\bar{\gamma}=(1-\gamma)(1-\delta) \tag{2.27b}$$
$$2\varepsilon_p(1-\gamma)[(1-\delta)+d_A^2+d_B^2]-2\varepsilon_p\,\bar{\gamma}(1-\delta)$$
$$=\Delta\sum_{\sigma}[\lambda_{\sigma}^{(-)}-\Delta(1-\gamma)]\,I_{\sigma}^{(0)}$$
$$-2\tau^2\rho^2\gamma\frac{\varepsilon_p}{\hbar\omega}\sum_{\sigma}q_{A\sigma}\,q_{B\sigma}\,I_{\sigma}^{(2)} \tag{2.27c}$$

$$\frac{\hbar\omega}{4}(1-\tau^{-4})=\gamma^2\rho^2\frac{\varepsilon_p}{\hbar\omega}\sum_{\sigma}q_{A\sigma}\,q_{B\sigma}\,I_{\sigma}^{(2)}. \tag{2.27d}$$

In the above equations, we use the abbrevations

$$I_{\sigma}^{(0)}:=\frac{1}{N}\sum_{\mathbf{k}\nu}n_{\mathbf{k}\nu\sigma}\frac{1}{\varepsilon_{\mathbf{k}\nu\sigma}}, \tag{2.28a}$$

$$I_{\sigma}^{(2)}:=\frac{1}{N}\sum_{\mathbf{k}\nu}n_{\mathbf{k}\nu\sigma}\frac{\varepsilon_k^2}{\varepsilon_{\mathbf{k}\nu\sigma}}, \tag{2.28b}$$

$$x_{\eta\sigma}:=e_{\eta}\,p_{\eta\sigma}+p_{\eta-\sigma}\,d_{\eta}, \tag{2.28c}$$
$$\delta_{\eta\sigma}:=1/2-p_{\eta\sigma}^2-d_{\eta}^2, \tag{2.28d}$$

as well as the conventions $\xi_{\eta}=1(-1)\Leftrightarrow\eta=A(B)$ and $\sigma=1(-1)\Leftrightarrow\sigma=\uparrow(\downarrow)$.

Furthermore, we introduce the charge (Δ_{CDW}) and spin density wave (Δ_{SDW}) order parameters

$$\Delta_{\mathrm{CDW}}=\frac{1}{2}(n_A-n_B)=\frac{1}{2}\sum_{\eta\sigma}\xi_{\eta}\,n_{\eta\sigma}=\frac{\Delta}{2\varepsilon_p(1-\gamma)}, \tag{2.29a}$$

$$\Delta_{\mathrm{SDW}}=\frac{1}{2}(m_A-m_B)=\frac{1}{2}\sum_{\eta\sigma}\xi_{\eta}\,\sigma\,n_{\eta\sigma}, \tag{2.29b}$$

and the net magnetization

$$m=\frac{1}{2}(m_A+m_B)=\frac{1}{2}\sum_{\eta\sigma}\sigma\,n_{\eta\sigma}, \tag{2.30}$$

where the sublattice particle numbers (per spin) and magnetizations are given by

$$n_{\eta}=1-\delta_{\eta}=n_{\eta\uparrow}+n_{\eta\downarrow}, \tag{2.31a}$$

$$n_{\eta\sigma}=\frac{1}{2}-\delta_{\eta\sigma}=p_{\eta\sigma}^2+d_{\eta}^2, \tag{2.31b}$$

and

$$m_{\eta}=n_{\eta\uparrow}-n_{\eta\downarrow}, \tag{2.32}$$

respectively. Finally, we define the local magnetic moment m_{loc} and the effective hopping amplitude t_{eff} [60] according to:

$$m_{\mathrm{loc}}=\frac{3}{8}\sum_{\eta}(n_{\eta}-2d_{\eta}^2), \tag{2.33}$$

$$t_{\mathrm{eff}}=\frac{\langle\sum c_{i\sigma}^{\dagger}\,c_{j\sigma}\rangle}{\langle\sum c_{i\sigma}^{\dagger}\,c_{j\sigma}\rangle_{U,\,\varepsilon_p,\,\omega=0}}. \tag{2.34}$$

2.3.3. *The adiabatic and the anti-adiabatic limits.* We have already mentioned that the variational ansatz (2.8) pro-

vides an interpolation scheme with respect to the variation of the phonon frequency ω. In this subsection we briefly discuss the both extreme limits $\omega \to 0$ and $\omega \to \infty$.

First we consider the adiabatic limit. Depending on coupling strength ε_p and particle density n, we have two types of solutions of (2.22–2.27):

$$\begin{aligned} &\text{I}: \gamma \propto \hbar\omega, \quad \tau^2 = \tau_c^2, \quad \rho = 1; \\ &\text{II}: \gamma = 1, \quad \tau^2 = 1, \quad \rho = 0. \end{aligned} \tag{2.35}$$

Increasing ε_p we obtain an abrupt transition from the state I to the perfectly localised self-trapped state II. Note that between regimes I and II a third solution may appear which is characterized by $\tau^2 \propto \hbar\omega \to 0$ as $\omega \to 0$ and $\rho_c < \rho \leqq 1$. This solution yields also a finite zero-point energy of phonons and a vanishing variance of the ion coordinates within the uncertainty principle in its minimal form. For the paramagnetic uncorrelated model (2.14), where $\Delta \equiv 0$ and the effective interaction term is taken in Hartree-Fock approximation, the domains of stability of the different solutions were analyzed in detail by the authors in [26]. Of course, for $U_{\text{eff}} > 0$ and $\Delta \neq 0$, the stability regions have to be determined numerically as function of ε_p and n. In this work, we will restrict us to the case of moderate EP coupling, i.e. $\varepsilon_p/t \lesssim 2$. Then we are able to show that $\bar{\gamma} = 1$, $\gamma = 0$, $\rho = 1$ and $0 < \tau_c^2 \leqq 1$ hold $\forall n$ at $\omega = 0$. In this regime, the adiabatic limit of our theory reproduces the results obtained in [44, 45].

For the nonadiabatic limit ($\omega \to \infty$, $\varepsilon_p/\hbar\omega \to 0$), we obtain $\gamma = \tau^2 = 1$ which implies $\bar{\gamma} = \Delta = 0$ and $\rho = 1$ for any choice of the model parameters. Thus the effective Hamiltonian (2.14) becomes the usual Hubbard Hamiltonian with $U_{\text{eff}} = U - 2\varepsilon_p$.

3. Numerical results and discussion

In the numerical evaluation of the self-consitency loop (2.23–2.28) we proceed as follows: eliminating the variables e_η^2, $p_{\eta\sigma}^2$, $\lambda_\eta^{(1)}$ and $\bar{\gamma}$, we solve the six remaining saddle-point equations for d_η^2 and $\lambda_\sigma^{(\pm)}$ together with the integral equation for μ (2.25) using an iteration technique. At given model parameters ε_p, U, ω and n (in the following all energies are measured in units of t, and $\hbar = 1$) this is done for a fixed initial set of variational parameters $\{\Delta^{(i)}, \gamma^{(i)}, \tau^{2(i)}\}$. Then, in an outer loop, the new set $\{\Delta^{(i+1)}, \gamma^{(i+1)}, \tau^{2(i+1)}\}$ is obtained from a fixpoint iteration of the variational equations (2.27a, c, d) at the point where the bosonic fields are stationary. Convergence is achieved if order and variational parameters are determined with relative error $\leqq 10^{-6}$. In this process, the **k**-summations were performed at $T = 0$ using the unperturbed 2D tight-binding density of states $N(\varepsilon) = K(1 - \varepsilon^2/16)/2\pi^2$, where $K(m)$ denotes the complete elliptic integral of the first kind. Note that our numerical procedure allows for the investigation of metastable solutions, which correspond to different symmetry broken states. Therefore, in the final analysis, the physically relevant saddle point is determined to give the lowest free energy (2.22).

The theory developed so far allows the investigation of the whole parameter range of EP coupling strengths. As already mentioned before, we will restrict the numerical calculations in the present work to the case of moderate EP interaction, where polaronic effects lead only to a weak mass renormalization of the charge carriers, i.e., we consider the "light" polaron regime. Since the critical coupling strength for the transition from "light" to "heavy" polarons was found to be $\varepsilon_{p,c}(n)/t \sim 4$–$6$ for the HHM [26], we chose as a typical EP coupling $\varepsilon_p = 1.8$ throughout this paper.

3.1. *Special limits of the Holstein-Hubbard model*

3.1.1. *The adiabatic limit* $\omega = 0$. First we recapitulate the basic features of the ground-state phase diagram of the HHM at $\omega = 0$ [45]. The domains of stability of several homogeneous ground states are shown in Fig. 1 in the $U - \delta$ plane. Here the different phases are classified according to the order parameters (2.29–2.30). For the states with vanishing net magnetization ($m = 0$) we have:

$$\begin{aligned} &\text{PM} \quad \Delta_{\text{CDW}} = 0 \quad \Delta_{\text{SDW}} = 0 \\ &\text{PM/CDW} \quad \Delta_{\text{CDW}} \neq 0 \quad \Delta_{\text{SDW}} = 0 \\ &\text{AFM} \quad \Delta_{\text{CDW}} = 0 \quad \Delta_{\text{SDW}} \neq 0. \end{aligned}$$

The various FIM states ($m \neq 0$) can be specified with respect to the relative importance of SDW and CDW correlations (cf. [45]):

$$\begin{aligned} &\text{FIM} \quad \Delta_{\text{CDW}} \approx \Delta_{\text{SDW}} \\ &\text{FIM/SDW} \quad \Delta_{\text{CDW}} \ll \Delta_{\text{SDW}} \\ &\text{FIM/CDW} \quad \Delta_{\text{CDW}} \gg \Delta_{\text{SDW}}. \end{aligned}$$

(For the pure Hubbard model, away from half-filling, FIM solutions were considered first by Oleś [61] using the Local ansatz [62]). Additionally there is the FM state with $m > 0$ and $\Delta_{\text{CDW}} = \Delta_{\text{SDW}} = 0$.

At half-filling we obtain a stable PM/CDW state below a critical Hubbard interaction U_c, where the "dimeri-

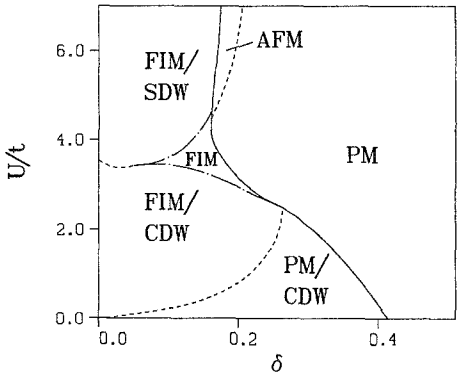

Fig. 1. Ground-state phase diagram of the 2D Holstein-Hubbard model in the adiabatic limit ($\omega = 0$) at $\varepsilon_p = 1.8$. The solid line separates states with finite lattice distortion from "undimerized" states. For further explanation see text

zation" of the square lattice is related via (2.29a) to the CDW order parameter. Increasing the Coulomb interaction the gap parameter Δ decreases up to the abrupt breakdown at the first-order transition to the AFM state. Note that U_c is only slightly reduced from its Hartree-Fock value $U_c^{HF}=2\varepsilon_p$ [44].

Off half-filling the situation becomes much more complex. Searching for saddle-point solutions one has to include, in principle, other symmetry-broken structures such as incommensurate CDW and SDW, or inhomogeneous phase separated structures as well. However, to keep the problem tractable in view of the additional EP coupling effects, we only consider commensurate $A-B$ structures. Solutions with finite Peierls distortions are lowest in energy for a large parameter range of U and δ. Depending on the relative strength U/ε_p one observes a CDW or SDW dominated regime. The dashed phase boundary between FIM/CDW and FIM/SDW denotes a first-order transition, whereas both Δ_{CDW} and Δ_{SDW} vary continuously along the FIM/CDW⇌FIM⇌FIM/SDW transition. It has to be noted that the FM state is absent within this parameter range.

3.1.2. *The case* $U_{eff}=0$. At finite frequencies, the effective Coulomb repulsion $U_{eff}=U-2\varepsilon_p(2\gamma-\gamma^2)$ is reduced by polaronic effects. In particular, for $U<2\varepsilon_p$, an attractive interaction $U_{eff}<0$ appears at high enough frequencies. It is just this phenomenon which gives rise to the possibility of bipolaron formation. In the standard polaron theories, the interaction term is usually neglected. This is certainly correct in the extreme dilute limit $n\ll 1$. However, at finite electron densities the effective electron interaction becomes important. Putting U_{eff} equal to zero before the variation of the ground-state energy (2.22) with respect to $\bar{\gamma}$, γ, τ^2 and d^2, we obtain, e.g., for the small polaron transition an unphysical large critical coupling strength $\varepsilon_{pc}\propto(1-n)^{-1}$ near half-filling [26].

The approximation $U_{eff}\equiv 0$ was used by Weber et al. [63] to investigate electronic correlations in Peierls systems. The main problem of this approach lies in the fact, that the advantage of an exact diagonalization of the transfomed Hamiltonian (which is strictly valid only for one special point in the parameter space), is accompanied by a loss of variational degrees of freedom.

To determine the hyperplane where $U_{eff}=0$ is actually fulfilled, we solve the complete set of self-consistency (2.26–2.27), ensuring the constraint

$$\gamma_0=1-\sqrt{1-\frac{U}{2\varepsilon_p}}. \tag{3.36}$$

Then the extremal free energy is obtained as

$$f(U_{eff}=0)=\frac{\hbar\omega}{4}(\tau_0^2+\tau_0^{-2})+\frac{\Delta^2}{4\varepsilon_p}-\varepsilon_p n[1-(1-n)(1-\gamma_0)^2]$$
$$+\frac{2}{N}\sum_{\mathbf{k}\nu}\nu\sqrt{\Delta_0^2(1-\gamma_0)^2+\rho_0^2\varepsilon_{\nu\mathbf{k}}^2}\,\Theta(\varepsilon_F-\varepsilon_{\nu\mathbf{k}}). \tag{3.37}$$

Figure 2 shows the corresponding ($U_{eff}=0$) contourplot as function of U in the $\omega-\delta$ plane at $\varepsilon_p=1.8$. The solid line separates the Peierls distorted state from the pure PM. In the nonadiabatic limit ($\omega\to\infty$) the "dimerization" vanishes asymptotically even at $\delta=0$ where $U_{eff}=0$ is reached for $U=2\varepsilon_p$ independent of δ. Figure 2 indicates clearly that, including even a weak Hubbard interaction, bipolaron formation becomes unlikely in the low-frequency regime.

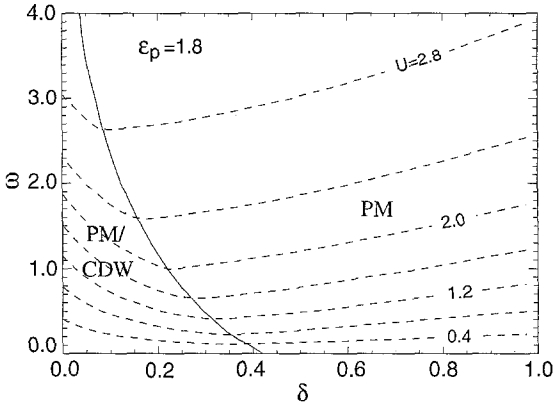

Fig. 2. Lines of constant U on the $U_{eff}=0$ hyperplane

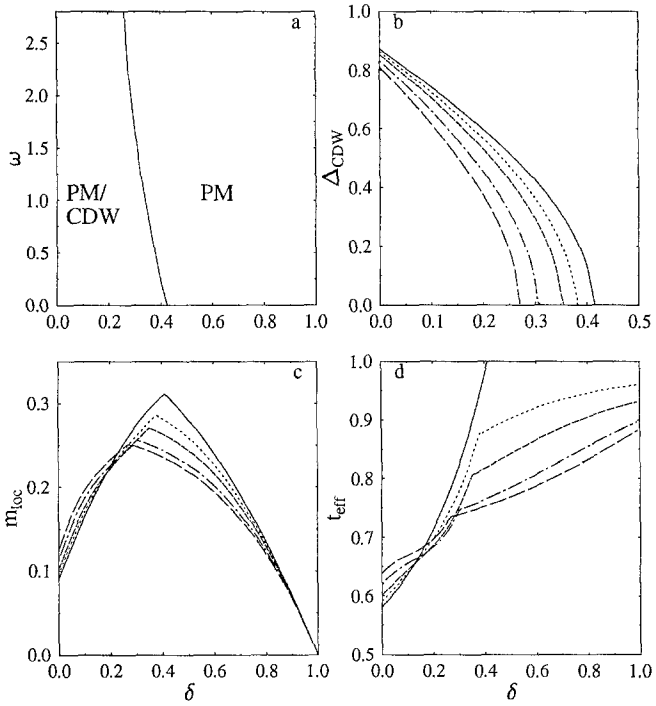

Fig. 3. Phase diagram of the pure Holstein model ($U\equiv 0$), CDW order parameter Δ_{CDW}, local magnetic moment m_{loc}, and effective hopping amplitude t_{eff} are shown as a function doping δ in **a**, **b**, **c** and **d**, respectively. The results are given at $\varepsilon_p=1.8$ for various phonon frequencies $\omega=0$ (full), 0.4 (dotted), 0.8 (dashed), 1.6 (chain dotted), and 2.4 (long dashed)

3.1.3. *The pure Holstein model.* In proceeding to investigate the solution of the extremal equations (2.26) and (2.27), it is useful to consider first the special case $U=0$, i.e. the Holstein model. Our numerical results are summarized in Figs. 3 and 4.

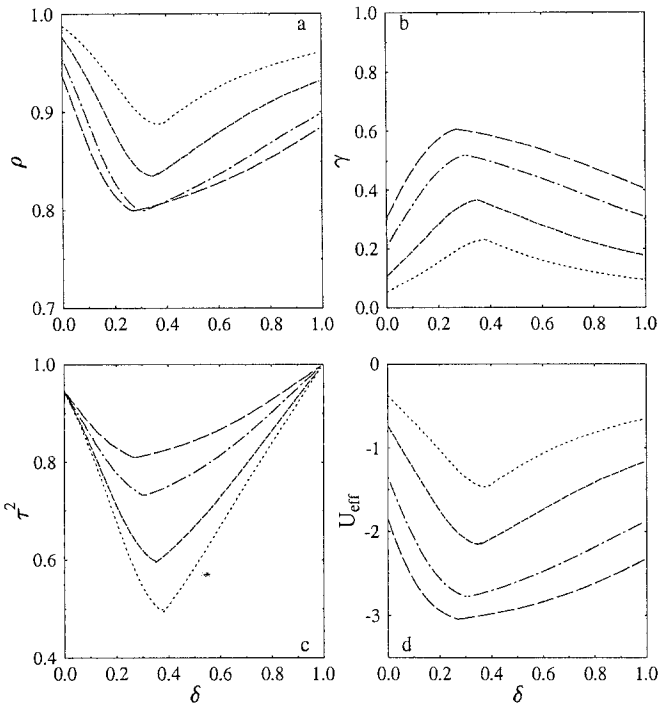

Fig. 4. Polaron band narrowing ρ **a**, polaron γ **b** and squeezing τ^2 **c** variational parameters, as well as the effective Coulomb interaction U_{eff} **d** as function of doping at various frequencies. The notation is the same as in Fig. 3a–d

The stability region of the state with finite Peierls distortion is shown in Fig. 3a. Doping the system away from half-filling, a second-order phase transition PM/CDW⇌PM takes place, where the transition point $\delta_c(\omega)$ is shifted to lower values increasing the phonon frequency. To analyze this transition and the main features of the ground-state solution, in Fig. 3b–d we present Δ_{CDW}, m_{loc} and t_{eff} as a function of doping at various frequencies. As can be seen from Fig. 3b, the CDW order parameter goes continuously to zero with increasing δ. Let us emphasize that the static Peierls distortion is suppressed by two effects acting in combination. The δ-effect, which exists at $\omega=0$ as well, can be attributed to an increasing asymmetry in the occupation numbers d_A^2 and e_B^2 upon doping (recall that the on-site energies are lowered (raised) on the A (B)-sublattice in the CDW state, thus one has $d_A^2=e_B^2>d_B^2=e_A^2$ at half-filling). The inclusion of phonon dynamics yields a further reduction of the CDW long-range order. Obviously, the finite-ω effects, which in our variational approach are mainly realized via the ability to polaron formation, become more important at larger hole concentrations. The destruction of the PM/CDW structure leads to the occurence of a larger number of single occupied sites and therefore to an enhancement of the local magnetic moment (see Fig. 3c; m_{loc} can be viewed as a measure for the "localization" of the electronic spin). At the same time, the mobility of the charge carries is increased, so we get a considerably enhanced effective hopping amplitude t_{eff} (cf. Fig. 3d). Clearly, in the PM state, one observes with decreasing electron density a decrease (increase) of m_{loc} (t_{eff}).

For a more detailed discussion of the non-diabatic effects, in Fig. 4a–d we have plotted the polaron band narrowing (ρ), the variational parameters γ and τ^2, and the effective interaction U_{eff}. First of all, as displayed in Fig. 4b, the main effect of the quantum fluctuations is to enhance the tendency towards polaron formation. That means, the movement of the charge carriers and its concomitant lattice distortion creates large anomalous fluctuations of the lattice coordinates and the local charge density. It follows that the (adiabatic) CDW ordering is decreased with respect to the case $\omega=0$ (cf. the interference term $\propto(-1)^i\Delta(1-\gamma)$ in (2.19)). As pointed out by Feinberg et al. [39], in a many-polaron system, the coherent motion of polarons implies by a quantum-mechanical effect a squeezing of the conjugated momentum fluctuations which counteracts the polaronic band renormalization (Fig. 4c). Including this squeezing phenomena, the net result for ρ is shown in Fig. 4a. Let us stress that our variational treatment yields a rather weak polaron band narrowing ($\rho\sim 0.8$–$0.9\ \forall\delta$ compared to $\rho\sim 10^{-4}$ in the normal small polaron theory [29]), i.e. even for $\varepsilon_p/t\sim 2$–4 [26] the polarons are "light" quasiparticles. At low doping the loss of mobility due to the reduction of ρ is overcompensated by the gain of kinetic energy when the long-range order (CDW) goes down and t_{eff} increases with ω (cf. Fig. 3d). At larger (but fixed) δ, i.e. especially in the PM region, t_{eff} is reduced by the polaron band narrowing (note that now $t_{\text{eff}}(\omega=0)=1$ holds). Of course, for the Holstein model, the effective Hubbard interaction U_{eff} is always negative (Fig. 4d). This attractive on-site interaction would favour bipolaron formation if the electron-phonon coupling is strong enough ($\varepsilon_p/t\sim 3$ [64]). (Contrary to the CDW state the bipolaronic state may be characterized by an enhanced probability for double occupancy on *both* sublattices). In our coupling regime ($\varepsilon_p=1.8$), however, the probability of single occupancy becomes only somewhat weakened and as a result the local magnetic moment is slightly reduced with increasing ω (cf. Fig. 3c). Clearly, these correlation effects are of minor importance at low particle densities. Therefore, t_{eff} increases with δ. In the limit $\delta\to 1$, we have $\gamma=\hbar\omega/(\hbar\omega+4\rho t)$, $\tau^2=1$ and $t_{\text{eff}}=\rho$.

3.2. *Phase diagram of the Holstein-Hubbard model*

3.2.1. *The $\delta=0$ case.* At half-filling, the unperturbed 2D tight-binding band structure gives rise to perfect (π,π) Fermi surface nesting. Then, depending on the relative interaction strengths of ε_p and U, the system shows an instability towards the formation of a CDW or SDW (AFM) state modulated with the same wave vector.

The phase boundary between the PM/CDW and the AFM states, shown in Fig. 5a, was determined from the points of intersection of the corresponding free energies. The critical value U_c, where the first-order phase transition PM/CDW⇌AFM takes place, is approximately independent of ω ($U_c(\omega)\lesssim U_c^{\text{HF}}$). In the extreme anti-adiabatic limit, we obtain the Hartree-Fock result $U_c(\omega\to\infty)\to U_c^{\text{HF}}$. The dependence of the CDW(SDW) order parameter on the phonon frequency is displayed in

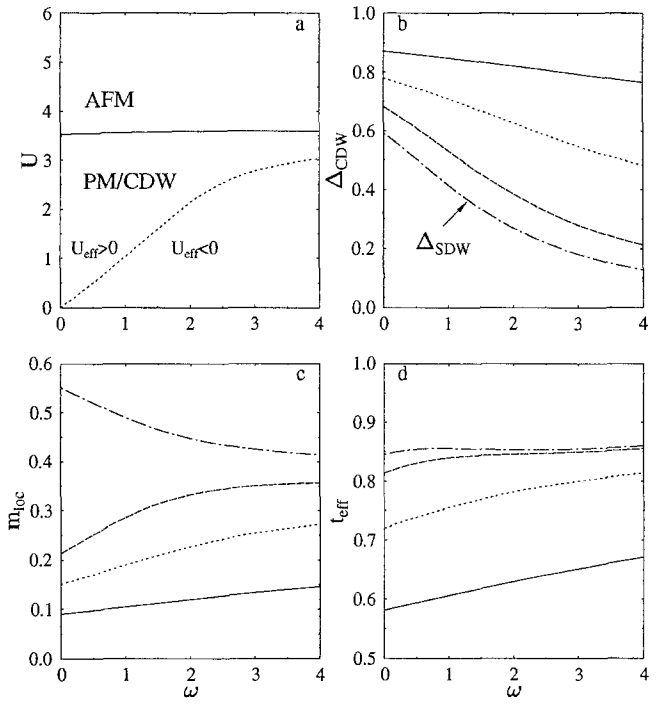

Fig. 5. a–d The domains of stability of AFM and PM/CDW states in the $U-\omega$ plane are depicted in **a** for the half-filled band case. The dotted line indicates the boundary $U_{eff}=0$. The CDW(SDW) order parameter Δ_{CDW} (Δ_{SDW}), the local magnetic moment m_{loc} and the effective hopping t_{eff} vs phonon frequency ω are given in **b**, **c** and **d** respectively. We show results for different values of Hubbard interaction $U=0$ (full), 2 (dotted), 3 (dashed), and 4 (chain dotted). The electron-phonon coupling is $\varepsilon_p=1.8$

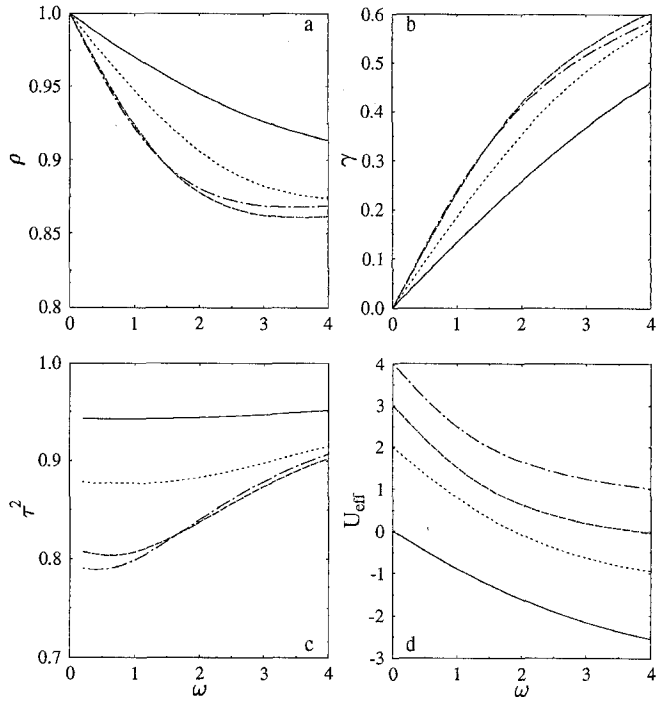

Fig. 6. Shown are the frequency dependencies of ρ **a**, γ **b**, τ^2 **c**, and U_{eff} **d** for the same model parameters as in Fig. 5

Fig. 5b for different characteristic Coulomb interaction strengths, which corresponds to CDW ($U=0, 2, 3$) and AFM solutions ($U=4$) at half-filling. Obviously, the long-range order is weakened when the frequency of the lattice vibrations is raised (cf. $\Delta_{CDW}(\omega)$ and $\Delta_{SDW}(\omega)$ in Fig. 5b). As a result the local magnetic moment goes down (up) in the CDW(AFM) phase (Fig. 5c). At fixed ω, the Peierls distortion becomes rapidly suppressed if the on-site Coulomb interaction is taken into account. Increasing U, the energy cost at double occupied sites starts to dominate the energy gain on one sublattice (A) through static "dimerization". At the same time we find, as seen in Figs. 5d, that the gain of kinetic energy ($\propto t_{eff}$) becomes more important until the AFM is established at U_c. Then, in the AFM phase, t_{eff} is a monotonous decreasing function of U as in the static case [44, 60].

Figure 6a–d shows the band narrowing factor ρ, the variational parameters γ and τ^2, and U_{eff} as a function of frequency for $U=0, 2, 3$ and 4. First of all, we obtain again a very modest polaronic band narrowing (Fig. 6a), even for sizeable values of γ, i.e. relative strong polaron effect (cf. Fig. 6b). This is in agreement with the previous findings for the 1D HHM [25]. At low frequencies, the optimum value of the variational parameter γ grows approximately linear with ω. As already stated, the non-adiabaticity in our system is mainly connected to the polaron effect. Thus, γ is a monotonically increasing function of ω [25]. Interpolating to the anti-adiabatic limit, one gets $\gamma(\omega\to\infty)=1$. Compared to the case $U=0$, in the CDW state, the polaron effect is enhanced increasing U. This is clearly related to the suppression of the CDW long-range order. In the AFM state, the U-dependence of γ is reversed.

The squeezing parameter τ^2 shows a non-monotonous behavior as function of ω (Fig. 6c). As remarked in Sect. 2.2, the squeezing phenomenon is most pronounced in the regime where $t\sim\omega\sim\varepsilon_p$. In this region the energy loss due to the enhanced zero-point energy of the phonon subsystem can be overcompensated by the gain of kinetic energy in the electronic (polaronic) system (squeezing of the momentum fluctuations). For $\omega\to\infty$ (anti-adiabatic limit [25]) as well as for very large couplings ($\varepsilon_p\gg t$; heavy polaron limit [26]) there is no squeezing effect ($\tau^2=1$). Figure 6d shows the reduction of the effective Hubbard interaction with increasing polaron effect. This tells us why, in the AFM state, Δ_{SDW} and m_{loc} goes down at higher frequencies (cf. Figs. 5b, c).

Summarizing this section, we reiterate the important point that our variational treatment of the phonon dynamics yields a significant ω-dependence of the polaronic (γ), squeezing (τ^2) and correlation (U_{eff}) effects. This should be contrasted to the results of the standard polaron theory [29, 37] where, of course, $\gamma\equiv1$, $\tau^2\equiv1$, and $U_{eff}=U-2\varepsilon_p$.

Finally, let us notice that Zheng et al. [25] have studied the effect of finite phonon frequency on the Peierls dimerization using a modified Gutzwiller approach for the HHM. However, their calculations are restricted to the half-filled band case, the PM/CDW state and one spatial dimension. In this limit, we are able

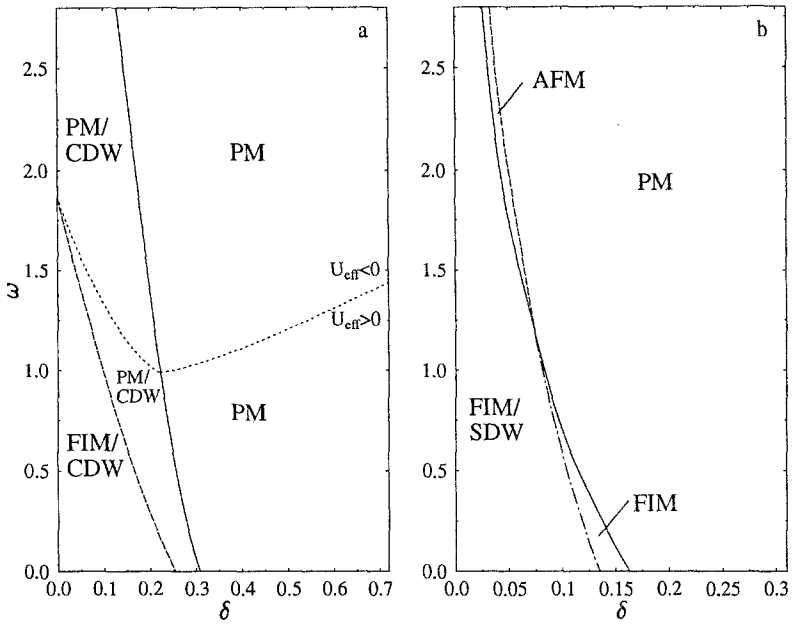

Fig. 7. The phase diagram of the Holstein-Hubbard model is displayed in the $\delta-\omega$ plane for $\varepsilon_p=1.8$ at $U=2$ **a** and $U=4$ **b**. Solid curves separate states with and without "dimerization"; dashed lines denote the phase boundaries between phases with different magnetic order. The chain dotted curve corresponds to the "transition" FIM/SDW⇌FIM (see text). In **a** the $U_{\text{eff}}=0$ line is marked by the dotted curve

to verify their numerical results within the framework of our variational SB scheme.

3.2.2. *The $\delta\neq 0$ case.* We now work out the finite ω-effects on the ground-state phase diagram of the 2D HHM (cf., the $\omega=0$ phase diagram presented in Sect. 3.1.1, Fig. 1). Analyzing the stability of the various homogeneous states by comparing the corresponding free energies, we obtain the shift of the phase boundaries as function of ω shown in Fig. 7. The results are given at two characteristic Hubbard interaction strengths $U=2$ (Fig. 7a) and $U=4$ (Fig. 7b), which, with respect to the ratio U/ε_p, refer to the CDW and SDW dominated region of the $\delta-U$ phase diagram (see Fig. 1), respectively. As reported in the previous section, at half-filling, we obtain a PM/CDW (AFM) state $\forall\omega$ at $U=2$ ($U=4$). Upon doping we observe a transition from states with finite static Peierls distortion (PM/CDM (a); FIM/SDW (b)) to "undimerized" states (PM (a); AFM, PM (b)) at a critical hole concentration $\delta_c(\omega)$. Increasing the frequency of the lattice vibrations this transition is shifted to lower values of δ_c, i.e., at high enough ω, the long-range order (CDW, SDW) is destroyed by quantum fluctuations connected to polaron formation and squeezing effects (see also the discussion in Sect. 3.1.3). In the FIM/CDW, FIM/SDW and FIM states both charge (driven by ε_p) and spin correlations (established by U_{eff}) coexist. Due to the additional weakening of the effective Coulomb interaction at higher frequencies, the states with FIM spin order become more suppressed than the states with PM/CDW order (cf. Fig. 7a). Note that the transitions accompanied by a change in both SDW and CDW order are first-order phase transitions (FIM/CDW ⇌PM/CDW; FIM/SDW⇌AFM, PM; FIM⇌PM), whereas the transitions PM/CDW, AFM⇌PM are of second order. In addition we would like to stress, that there is no sharp phase boundary between FIM/SDW and FIM states. We determined the transition line (chain dotted curve in Fig. 7b) from the somewhat arbitrary requirement $\Delta_{\text{CDW}}=\Delta_{\text{SDW}}$. Then this transition point also corresponds to a local maximum of t_{eff}. The dotted curve in Fig. 7 a shows the $U_{\text{eff}}=0$ line. Above $\omega_c=1.87$ (obtained in the limit $\delta\to 0$), we have $U_{\text{eff}}<0\ \forall\delta$, i.e., a magnetic solution (Δ_{SDW}, $m\neq 0$) doesn't exist. At fixed frequency ω, $U_{\text{eff}}(\delta)$ takes its minimal value at the transition point $\delta_c(\omega)$ where the polaron effect becomes strongest (see below).

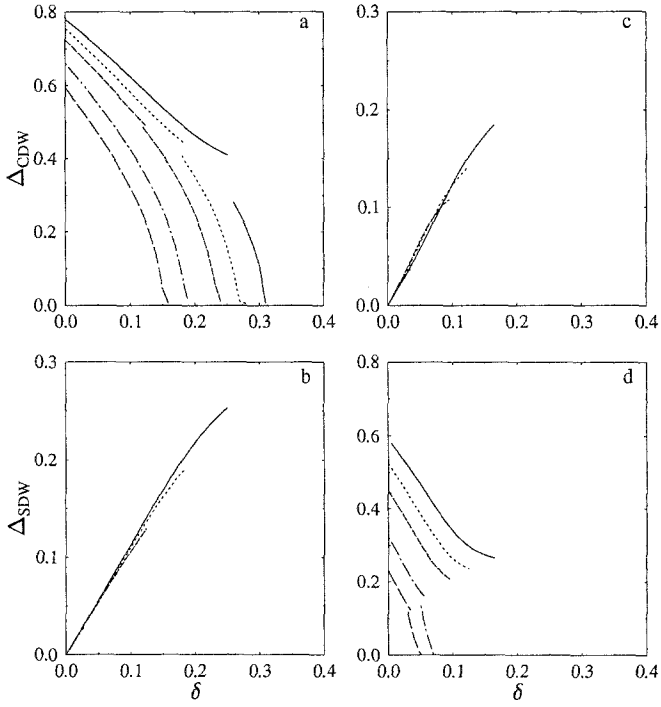

Fig. 8. Order parameters Δ_{CDW} and Δ_{SDW} are given as function of doping δ at $U=2$ (**a, b**) and $U=4$ (**c, d**), respectively. Results are shown for $\omega=0$ (full), 0.4 (dotted), 0.8 (dashed), 1.6 (chain dotted), and 2.4 (long dashed) at $\varepsilon_p=1.8$

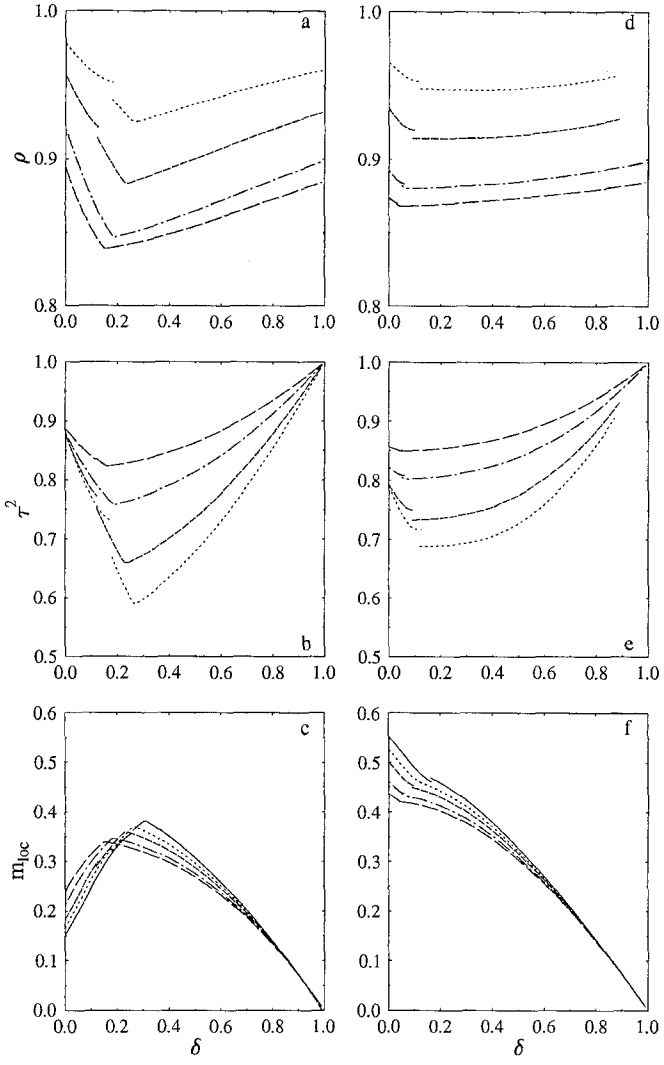

Fig. 9. The corresponding results for the polaron band narrowing ρ **a(d),** the squeezing effect **b(e),** and the local magnetic moment m_{loc} **c(f)** at $U=2(4)$. The notation is the same as in Fig. 8

The variation of the CDW and SDW order parameters is illustrated in Fig. 8 for the same interaction strengths $U=2$ (a, b) and $U=4$ (c, d) as in Fig. 7. Obviously, the behavior of Δ_{CDW} and Δ_{SDW} as function of doping is reversed as one moves from the CDW to the SDW region. For $U=2$ ($U=4$) we have $n_A \gg n_B$ ($m_A \gg |m_B|$), where the dominance of the CDW (SDW) correlations is most pronounced in the vicinity of the half-filled band case (note the different scales of the axis of ordinate in Fig. 8). In the FIM states the resulting net magnetisation (2.30) obeys the relation $m=\min(\delta, 1-\delta)$. Let us emphasize, that for large Hubbard interactions, i.e. in the SDW region, the EP coupling causes a monotonous increase of the CDW correlations (order parameter) doping the system away from half-filling. This result is supported by quantum MC [23] and exact diagonalization [11, 41] studies (of course, within our A – B saddle-point approximation, we are unable to describe *local* phonon-driven lattice distortions). As can be seen from Fig. 8, in the predominant CDW(SDW) ordered phases the static Peierls distortion (magnetic order) is strongly reduced with increasing ω, whereas $\Delta_{\mathrm{SDW}}(\Delta_{\mathrm{CDW}})$ shows only a weak ω-dependence. The jump-like behavior of Δ_{CDW} (a) and Δ_{SDW} (d) at certain $\delta_c(\omega)$ is related to an intersection of the free energies for the different phases indicating a first-order phase transition.

Figure 9 shows the δ-dependence of ρ, τ^2 and m_{loc} at different frequencies for $U=2$ (a–c) and $U=4$ (d–f), respectively. Again we observe a relative week polaron band renormalization $\rho \sim 0.9$ at a moderate EP coupling $\varepsilon_p=1.8$. This can be attributed to our variational treatment of polaron and squeezing effects. The minimum of $\rho(\delta)$ is connected to the transition to the "undimerized" PM state at $\delta_c(\omega)$. Since the electronic correlation ($\propto U$) becomes less important in the dilute limit (i.e. at large δ), in this region the behavior of ρ is dominated by EP and kinetic energy effects. Increasing the Coulomb interaction U at fixed EP coupling ($\varepsilon_p=1.8$) and phonon frequency ($\omega=0.8$), $\rho(U)$ raises up to a maximum at about $U_{\max}=2\varepsilon_c$, where $\varepsilon_c(\delta, \omega)$ denotes the critical EP coupling strength for the transition to the heavy polaron state [26, 64]. Above $U_{\max}$, we obtain a very smooth decrease of $\rho(U)$ driven by the electronic band renormalization ($\propto q_{\eta\sigma}$). The limit $U=\infty$ is discussed in more detail in [26]. As already mentioned, the squeezing phenomenon favors the quantum-mechanical tunneling of polarons and therefore enhances (suppresses) the itinerancy of the "polaronic" charge carriers (a static Peierls distortion). Figure 9b (e) shows that the effect of squeezing is most pronounced at the transition PM/CDW, FIM$\rightleftharpoons$PM. At $U=2$, the behavior of m_{loc} as function of δ and ω was found to be qualitatively similar to the results obtained for the Holstein model in Sect. 3.1.3. (cf. Figs. 3c and 9c). On the other hand, m_{loc} is strongly enhanced in the FIM/SDW phase and shows, compared to the FIM/CDW case, a reversed dependence on ω and δ (see Fig. 9c, f).

4. Summary

We conclude by summarizing the gist of our approach and the most important numerical results. This paper aims to address the nonadiabatic effects in a strongly coupled electron-phonon system described by the Holstein-Hubbard model. Thus the central goal was to work out a theory, which enables us to treat both electron-electron (U) and electron-phonon (ε_p) interaction over the whole range of coupling strength on an equal footing and which, with respect to the phonon frequency (ω), provides an interpolation scheme from the adiabatic ($\omega=0$) to the antiadiabatic ($\omega\rightarrow\infty$) limit. In a first step we have performed a variational squeezed-polaron transformation of the HHM to extract the phonon dynamics related to polaron and squeezing effects at arbitrary band-fillings ($n=1-\delta$). In addition, the possibility of static (frozen) lattice deformations (Peierls distortions) was taken into account. Then the effective polaronic Hubbard Hamiltonian, obtained in the transformed phonon vacuum state, was treated by means of a slave boson technique on the two-sublattice saddle-point level

of approximation. From the extensive numerical evaluation of the resulting self-consistency equations, we believe to get at least a qualitative understanding of the ground-state properties of the HHM. The main results of our investigations are the following.

(*i*) We have presented, to our knowledge for the first time, the ground-state phase diagrams of the 2D Holstein and Holstein-Hubbard models for a wide class of model parameters $(U, \omega; \delta)$, where the EP coupling was fixed to an intermediate value ($\varepsilon_p/t = 1.8$). At half-filling the Holstein coupling leads to a PM state with static (π, π) Peierls distortion. Incorporating the intraatomic part of the Coulomb interaction U, the "dimerization" is a monotoneous decreasing function of U up to the point U_c, where the first order transition to the AFM state takes place. With increasing frequency of the lattice vibrations the static lattice distortion is reduced. Off half-filling, the phase diagram becomes more complex. Depending on doping level and Coulomb interaction strength, we observe Peierls distorted states with predominant charge (FIM/CDW, $\Delta_{\mathrm{CDW}} \gg \Delta_{\mathrm{SDW}}$; PM/CDW $\Delta_{\mathrm{SDW}} = 0$) or magnetic (FIM/SDW, $\Delta_{\mathrm{CDW}} \ll \Delta_{\mathrm{SDW}}$) long-range order as well as AFM, FM and PM phases ($\Delta_{\mathrm{CDW}} = 0$).
(*ii*) In our approach, the main effect of phonon dynamics is to enhance the tendency towards polaron formation. As first pointed out by Zheng et al. [46], the interference between (adiabatic) frozen "dimerization" and (antiadiabatic) polaron effect plays a very important role, especially in the intermediate parameter region where the energy scales are not well separated. As a result, the CDW long-range order is suppressed by quantum fluctuations. Due to the additional polaronic renormalization of the Hubbard interaction, in the SDW region, the magnetic correlations are weakened as well.
(*iii*) Clearly, in the adiabatic limit the theory yields the results obtained recently by the authors from a frozen phonon approach to the HHM [44, 45]. In the opposite antiadiabatic limit, we have no static Peierls distortion and, provided that $\varepsilon_p < \varepsilon_c$ (i.e. $\rho(\omega \to \infty) = 1$) [26], the theory fits the SB phase diagram for the pure Hubbard model with $U_{\mathrm{eff}} = U - 2\varepsilon_p$.
(*iv*) At finite frequencies, the central point, we would like to emphasize, is the strong ω and δ dependence of polaron and squeezing effects. As a result also the CDW/SDW order parameters, the local magnetic moment and the effective Hubbard interaction show a large variation with ω and δ. Note that this behavior cannot be obtained within the frozen phonon [45] or standard Lang-Firsov approach [29].
(*v*) The variational treatment of polaron formation at finite carrier densities yields an uncomplete polaron effect, i.e. light polarons, even at considerable EP coupling strengths ($\varepsilon_p < 4t$). The effective polaron mass is determined self-consistently, where the polaron narrowing ($\propto \rho$) and the correlation induced narrowing ($\propto q_{\mathrm{A}\sigma}\, q_{\mathrm{B}\sigma}$) are coupled. The SB approach allows us to treat both weak- and strong-coupling regimes as well. This is important since the correlation effects depends on the ratio U_{eff}/ρ (instead on U/t for the pure Hubbard model) which varies, e.g., near the self-trapping transition ($\varepsilon_p \sim \varepsilon_c$) over three orders of magnitude.
(*vi*) The squeezing effect enhances the mobility of the polaronic charge carriers ($\propto t_{\mathrm{eff}}$) and tends to suppress the CDW long-range order. In addition, the self-trapping transition is shifted to higher EP couplings [26]. However, compared to the ρ-corrections obtained from the modified variational treatment of polaron formation, the incorporation of the squeezing phenomenon yields, roughly speaking, a much smaller effect in the order of 5–10 percent. In the "light" polaron regime the polaron and squeezing effects are most pronounced at the PM/CDW$\rightleftharpoons$PM transition point.

Let us now comment on some limitations of the present approach. First, we have restricted ourselves to homogeneous commensurate (A – B) structures. Away from half-filling, however, other symmetry-broken states like spiral phases [58] or incommensurate charge ordered states may exist. In addition, from the concave curvature of the free energy as function of particle density one gets evidence that phase separated states become important upon doping into a commensurate correlated-insulating state [67]. Next, at least for $U_{\mathrm{eff}} < 0$, the possibility of superconducting [65] and/or bipolaronic states [66] should be taken into account for the HHM. Finally, evaluating the functional integral at the saddle-point of the bosonized action the static approximation was used for the bosonic fields, whereas the phonon dynamics is incorporated via the transformation to the "polaronic" Hubbard Hamiltonian in an effective way. This is certainly correct if the polarons can be described in terms of dressed quasiparticles having a well-defined band dispersion. However, it is not obvious, whether this quasiparticle concept can be maintained $\forall \omega$ and especially in the heavy polaron limit [68]. Work along this lines, in particular concerning the incommensurate CDW structures and the $U_{\mathrm{eff}} < 0$ case, is in progress.

The authors would like to thank D. Ihle for numerous and stimulating discussions.

References

1. Bednorz, I.G., Müller, K.A.: Z. Phys. B **64**, 189 (1986)
2. Rice, T.M., Less, J.: Common Met. **164–165**, 1439 (1990); Batlogg, B.: Physica B **169**, 7 (1991); Emery, V.J.: Physica B **169**, 17 (1991); Fukuyama, H.: Physica C **185–189**, xxv (1991); Ginzburg, V.L.: Physica C **209**, 1 (1993)
3. Tsuda, N., Nasu, K., Yanese, A., Siratori, K.: Electronic Conduction in Oxides. Berlin, Heidelberg, New York: Springer 1990
4. Manh, D., Mayou, D., Cyrot-Lackmann, F.: Europhys. Lett. **13**, 167 (1990)
5. Friedl, B., Thomsen, C., Cordona, M.: Phys. Rev. Lett. **65**, 1990 (1990)
6. Güttler, B., Salje, E., Freeman, P., Blunt, J., Harris, M., Duffield, T., Ager, C.D., Hughes, H.P.: J. Phys. **2**, 8977 (1990); Litvinchuk, A.P., Thomson, C., Cordona, M., Stastny, P., Mateev, D.M.: Phys. Rev. B **44**, 9723 (1991)
7. Sharma, R.P., Rehn, L.E., Baldo, P.M., Lin, J.Z.: Phys. Rev. Lett. **62**, 2869 (1989); Haga, T., Yamaya, K., Abe, Y., Tajima, Y., Hidaka, Y.: Phys. Rev. B **41**, 826 (1990)
8. Egami, T., Toby, B.H., Billinge, S.J.L., Janot, Chr., Jorgenson, J.D., Hinks, D.G., Subramanian, M.A., Crawford, M.K.,

Farneth, W.E., McCarron, E.M.: In: Electronic Structure and Mechanisms of High Temperature Superconductivity. Ashkenazi, J., Barnes, S.E., Zuo, F., Vezzoli, G., Klein, B.M. (eds.) New York: Plenum Press 1991
9. Kim, Y.H., Foster, C.M., Heeger, A.J., Cox, S., Stucky, G.: Phys. Rev. B**38**, 6478 (1988)
10. Jorgenson, J.D.: Phys. Today **44**, 34 (1991)
11. Zhong, J., Schüttler, H.-B.: Phys. Rev. Lett. **69**, 1600 (1992)
12. Suzuki, Y.Y., Pincus, P., Heeger, A.J.: Phys. Rev. B**44**, 7127 (1991); Bi, X.-X., Eklund, P.C.: Phys. Rev. Lett. **70**, 2625 (1993)
13. Mustre de Leon, J., Batistić, I., Bishop, A.R., Conradson, S.D., Trugman, S.A.: Phys. Rev. Lett. **68**, 3236 (1992)
14. Alexandrov, A.S., Ranninger, J.: Phys. Rev. B**45**, 13109 (1992); Physica C**198**, 360 (1992)
15. Hirsch, J.E.: Phys. Rev. B**47**, 5351 (1993)
16. Emin, D.: In: Physics of High-Temperature Superconductors, Maekawa, S., Sato, M. (eds.) Berlin, Heidelberg, New York: Springer 1992; Phys. Rev. B**45**, 5525 (1992)
17. Verbist, G., Peeters, F.M., Devreese, J.T.: Phys. Scr. T**39**, 66 (1991)
18. Cohen, R.E., Pickett, W.E., Krakauer, H.: Phys. Rev. Lett. **64**, 2575 (1990); Krakauer, H., Pickett, W.E., Cohen, R.E.: Phys. Rev. B**47**, 1002 (1993)
19. Anisimov, V.I., Korotin, M.A., Zaanen, J., Andersen, O.K.: Phys. Rev. Lett. **68**, 345 (1992)
20. Ramšak, A., Horsch, P., Fulde, P.: Phys. Rev. B**46**, 14305 (1992)
21. Hirsch, J.E.: Phys. Rev. B**31**, 6022 (1985)
22. Jurczek, E., Rice, T.M.: Europhys. Lett. **1**, 225 (1986); Prětre, A., Rice, T.M.: J. Phys. C**19**, 1365 (1986); Prelovšek, P., Rice, T.M., Zhang, F.C.: J. Phys. C**20**, L229 (1987)
23. Muramatsu, A., Hanke, W.: Physica C**153**, 229 (1988)
24. Zheng, H.: Phys. Rev. B**41**, 4723 (1990)
25. Zheng, H., Feinberg, D., Avignon, M.: Phys. Rev. B**41**, 11557 (1990)
26. Fehske, H., Ihle, D., Loos, J., Trapper, U., Büttner, H.: Z. Phys. B (submitted for publication)
27. Das, A.N., Konior, J., Ray, D.K., Oleś, A.M.: Phys. Rev. B**44**, 7680 (1991)
28. Batistić, I., Gammel, J.T., Bishop, A.R.: Phys. Rev. B**44**, 13228 (1992)
29. Holstein, T.: Ann. Phys. **8**, 325 (1959); ibid. **8**, 343 (1959)
30. Hirsch, J.E., Fradkin, E.: Phys. Rev. B**27**, 4302 (1983)
31. Marsiglio, F.: Phys. Rev. B**42**, 2416 (1990)
32. Scalettar, R.T., Bickers, N.E., Scalapiono, D.J.: Phys. Rev. B**40**, 197 (1989); Noack, R.M., Scalapino, D.J., Scalettar, R.T.: Phys. Rev. Lett. **66**, 778 (1991); Vekić, M., Noack, R.M., White, S.R.: Phys. Rev. B**46**, 271 (1992); Noack, R.M., Scalapino, D.J.: Phys. Rev. B**47**, 305 (1993)
33. Levine, G., Su, W.P.: Phys. Rev. B **42**, 4143 (1990)
34. Aubry, S., Quemerais, P., Raimbault, J.: Proceedings of the Third European Conference on Low Dimensional Superconductors, (Dubrovnik, Yougoslavia 1989)
35. Suzuki, S., Toyozawa, Y.: J. Phys. Soc. Jpn. **59**, 2841 (1990)
36. Raedt, H.D., Lagendijk, A.: Phys. Rev. Lett. **49**, 1522 (1982)
37. Toyozawa, Y.: Prog. Theor. Phys. **26**, 29 (1961)
38. Emin, D.: Adv. Phys. **12**, 57 (1973)
39. Feinberg, D., Ciuchi, S., de Pasquale, F.: Int. J. Mod. Phys. B**4**, 1317 (1990)
40. Ranninger, J., Thibblin, U.: Phys. Rev. B**45**, 7730 (1992)
41. Fehske, H., Röder, H., Mistriotis, A., Büttner, H.: J. Phys. **5**, 3565 (1993); Röder, H., Fehske, H., Büttner, H.: Phys. Rev. B**47**, 12420 (1993)
42. Das, A.N., Konior, J., Ray D.K.: Physica C**170**, 215 (1990)
43. Schmeltzer, D., Bishop, A.R.: Europhys. Lett. **12**, 369 (1990)
44. Fehske, H., Deeg, M., Büttner, H.: Phys. Rev. B**46**, 3713 (1992)
45. Deeg, M., Fehske, H., Büttner, H.: Z. Phys. B**88**, 283 (1992); ibid. **91**, 31 (1993)
46. Zheng, H., Feinberg, D., Avignon, M.: Phys. Rev. B**39**, 9405 (1989)
47. Kotliar, G., Ruckenstein, A.E.: Phys. Rev. Lett. **57**, 1362 (1986)
48. Alexandrov, A.S.: Phys. Rev. B**38**, 925 (1988)
49. Lang, I.G., Firsov, Y.A.: Zh. Eksp. Teor. Fiz. **43**, 1843 (1962)
50. Zheng, H.: Solid State Commun. **65**, 731 (1988); Phys. Rev. B**37**, 7419 (1988); ibid. **38**, 11865 (1988)
51. Yuen, H.P.: Phys. Rev. A**13**, 2226 (1976)
52. Lo, C.F., Sollie, R.: Phys. Lett. A**169**, 91 (1992); Phys. Rev. B**48**, 10183 (1993)
53. Nasu, K.: Phys. Rev. B**35**, 1748 (1987)
54. Barnes, S.E.: J. Phys. F**6**, 1375 (1976)
55. Frésard, R., Wölfle, P.: Int. J. Mod. Phys. B**5&6**, 685 (1992)
56. Negele, J.W., Orland, H.: Quantum Many-Particle Systems. Reading, Mass: Addison-Wesley 1988
57. Li, T., Wölfle, P., Hirschfeld, P.J.: Phys. Rev. B**40**, 6817 (1989)
58. Frésard, R., Dzierzawa, M., Wölfle, P.: Europhys. Lett. **15**, 325 (1991); Doll, K., Dzierzawa, M., Frésard, R., Wölfle, P.: Z. Phys. B**90**, 297 (1993); Arrigoni, E., Strinati, G.C.: Phys. Rev. B**44**, 7455 (1991)
59. Rasul, J.W., Li, T.: J. Phys. C**21**, 5119 (1988); Lavagna, M.: Phys. Rev. B**41**, 142 (1990); Jolicoeur, T., Guillou, J.C.L.: Phys. Rev. B**44**, 2403 (1991)
60. Lilly, L., Muramatsu, A., Hanke, W.: Phys. Rev. Lett. **65**, 1379 (1990); The authors have performed a comparative study of the two-sublattice SB mean-field theory and quantum MC calculations, where an excellent agreement was obtained for ground-state energy, local magnetic moment and effective hopping matrix element
61. Oleś, A.M.: J. Phys. C**15**, L1065 (1982)
62. Stollhoff, G., Fulde, P.: Z. Phys. B**26**, 257 (1977)
63. Weber, S.: Thesis, Universität Bayreuth 1985; Weber, S., Büttner, H.: J. Phys. C**17**, L337 (1984)
64. Trapper, U. (unpublished)
65. Sofo, J.O., Balseiro, C.A.: Phys. Rev. B**45**, 377 (1992)
66. Micnas, R., Ranninger, J., Robaszkiewicz, S.: Rev. Mod. Phys. **62**, 113 (1990)
67. Emery, V.J., Kivelson, S.A.: Physica C**209**, 597 (1993)
68. Ranninger, J., Thibblin, U.: Phys. Rev. B**45**, 7730 (1992)